metals

MDPI

Article

Laves Phase Precipitation Behavior in HiperFer (High Performance Ferritic) Steel with and without Boron Alloying

Jana Pöpperlová [1], Daniela Wipp [1], Bernd Kuhn [2,*,†] and Wolfgang Bleck [1]

[1] Steel Institute, RWTH Aachen University (IEHK), Intzestr. 1, 52072 Aachen, Germany
[2] Institute of Energy and Climate Research (IEK), Microstructure and Properties of Materials (IEK-2), Forschungszentrum Jülich GmbH, 52425 Jülich, Germany
* Correspondence: bernd.kuhn@hs-rm.de; Tel.: +49-6142-898-4512
† Current address: Hochschule RheinMain, Faculty of Engineering, Am Brückweg 26, 65428 Rüsselsheim, Germany.

Abstract: High-chromium ferritic stainless HiperFer steels were developed for high-temperature applications in power conversion equipment. The presented research describes the precipitation behavior of the Laves phase after the thermomechanical treatment of Fe-17Cr-0.6Nb-2.4W HiperFer alloys with and without the addition of 55 ppm boron. The boron-alloyed variant was produced with the aim of enhancing grain boundary strengthening and consequently increasing creep resistance. The focus is set on the effect of boron on the thermomechanically induced precipitation of $(Fe,Cr,Si)_2(Nb,W)$ Laves phase at grain boundaries. The addition of boron modifies the diffusion conditions in the area of grain boundaries. Consequently, the formation of Laves phase is promoted and the particle growth and coarsening process are suppressed. The impact of boron addition was validated by performing creep and thermomechanical fatigue testing in the standard processing state of HiperFer steel. In the B-alloyed variant, increased creep ductility through the modification of the particle-free zone widths at high-angle grain boundaries was encountered. Nevertheless, an optimized thermomechanical treatment is necessary to fully utilize the increased ductility effect for the creep strength optimization of the B-alloyed grade.

Keywords: high-chromium ferritic steel; boron; intermetallic phase; precipitation

Citation: Pöpperlová, J.; Wipp, D.; Kuhn, B.; Bleck, W. Laves Phase Precipitation Behavior in HiperFer (High Performance Ferritic) Steel with and without Boron Alloying. *Metals* **2023**, *13*, 235. https://doi.org/10.3390/met13020235

Academic Editor: Angelo Fernando Padilha

Received: 6 December 2022
Revised: 19 January 2023
Accepted: 21 January 2023
Published: 26 January 2023

1. Motivation and Introduction

Single-phase, Laves phase-strengthened, HiperFer (High-Performance Ferritic) steels with a chromium content of 17 wt. % exhibit excellent oxidation and creep resistance for high-temperature applications in future thermal energy conversion and storage systems at an increased operating temperature of up to 650 °C. The desired high-temperature properties are achieved through the solid solution and Laves phase-precipitation-strengthening effects [1,2]. The formation of the strengthening intermetallic Laves phase $(Fe,Cr,Si)_2(W,Nb)$ is promoted with the optimized alloying of tungsten, niobium, and silicon. HiperFer steels are typically produced solely utilizing conventional thermal processes [3]. This process contains time-consuming, two-step tempering to achieve nucleation and growth of the desired Laves phase particles. Therefore, a significantly more time-efficient and economical thermomechanical manufacturing process was developed [4–6], achieving rapidly occurring thermomechanically induced Laves phase precipitation, which is used in this paper as well.

The improved creep strength is achieved by an increased volume fraction of the strengthening Laves phase particles in the grain interior as well as a complete occupation of the grain boundaries [2,7,8]. Creep deformation is substantially determined by the coarsening of the Laves phase particles. Creep damage and failure are generally attributed to grain boundaries and the accumulated plastic deformation in the particle-free zones located next to the grain boundaries [9,10]. In general, broad precipitate-free zones have a

negative impact on the mechanical properties and lifetime of the material [11,12]. Due to the absence of particles, these zones are softer than the surrounding precipitation-hardened matrix. Plastic deformation is concentrated in these zones along the grain boundaries, increasing the risk of grain boundary fracture. However, a positive effect of precipitate-free zones on ductility has been observed in highly precipitation-strengthened alloys [13,14]. This can be explained by specific dislocation processes. Sufficient minimum width of the precipitate-free zones allows slip and cross-slip of dislocations to a high degree and thus convey a uniform deformation of adjacent grains [12].

To further improve the high-temperature properties of the HiperFer steel class, research was conducted at RWTH Aachen, IEHK, and Forschungszentrum Jülich, IEK-2, and continuous optimizations of the chemical composition were applied [2,9,15–17]. To inhibit the coarsening tendency of the grain boundaries strengthening particles as well as the grain growth and, therefore, further improve the creep resistance in heat-resistant steels, it is stated that the addition of boron can be used [18–20]. Furthermore, it has been reported that grain boundary segregation of boron additionally promotes the precipitation on the grain boundaries resulting in a higher number density of fine precipitates [18,21]. The HiperFer steel alloy design is based on the practical absence of nitrogen and carbon addition, supporting the Laves phase precipitation by preventing the formation of niobium, tungsten, and chromium carbides, nitrides, or carbonitrides [5,15]. Therefore, no nitrogen (<0.001 wt. %) and no carbon (<0.01 wt. %) are present in the chemical composition. Correspondingly, no formation of boron nitrides or incorporation of boron into carbides occurs and the availability of boron for microstructure stabilization is ensured.

In this study, two high-purity HiperFer steels were used in order to investigate the inherent precipitation behavior of the Laves phase. The objective of this study was to clarify the impact of the addition of 55 ppm boron on the thermomechanically induced Laves phase precipitation, especially at the grain boundaries.

2. Materials and Experimental Methods

2.1. Material Preparation

Two 80 kg HiperFer stainless steel batches (Fe-17Cr-0.6Nb-2.4W), without boron (B0) and with the addition of 0.0055 wt. % boron (B55), were investigated in the present study. The materials were melted in a 2 kHz vacuum induction furnace and cast, followed by air cooling, at RWTH Aachen, IEHK. Afterward, the material was homogenized for two hours at 1200 °C and hot forged. Subsequently, the material was dissolution-annealed for 10 min at 1150 °C. Dissolution annealing is necessary to achieve a precipitation-free ferritic microstructure prior to processing. The chemical composition of these two HiperFer stainless steels is listed in Table 1. The carbon and nitrogen contents were analyzed by Thermal Carrier Gas Extraction (TGHE) utilizing a LECO TruSpec® Micro instrument (LECO Corporation, St. Joseph, Michigan, USA). Based on the chemical composition, thermodynamic calculations of equilibrium phases were performed using ThermoCalc simulation software (Database TCFE8).

Table 1. Chemical composition in wt. % of the investigated alloys.

Alloy	C	N	Si	Mn	Cr	Nb	W	B	Fe
B0	<0.01	<0.01	0.27	0.19	16.8	0.64	2.41	-	bal.
B55	<0.01	<0.01	0.30	0.20	16.8	0.62	2.35	0.0055	bal.

Laves phase precipitation induced by thermomechanical treatment was investigated based on the thermomechanical processing chain of HiperFer steels [4,5]. The trial treatments for the in-depth investigations into the thermomechanically induced precipitations were performed by applying a DIL-805A/D dilatometer from TA Instruments (Hüllhorst, Germany) utilizing cylindrical dilatometer samples (ø 5 × 9 mm^3) by varying the deformation temperatures (800/850/900 °C) and deformation grades (0.25/0.5/1). All further

parameters, such as heating rate (100 °C·min^{-1}), deformation rate (10 s^{-1}), and cooling rate (150 °C·s^{-1}), were held constant. The provided time–temperature process route as a part of the processing chain is depicted in Figure 1.

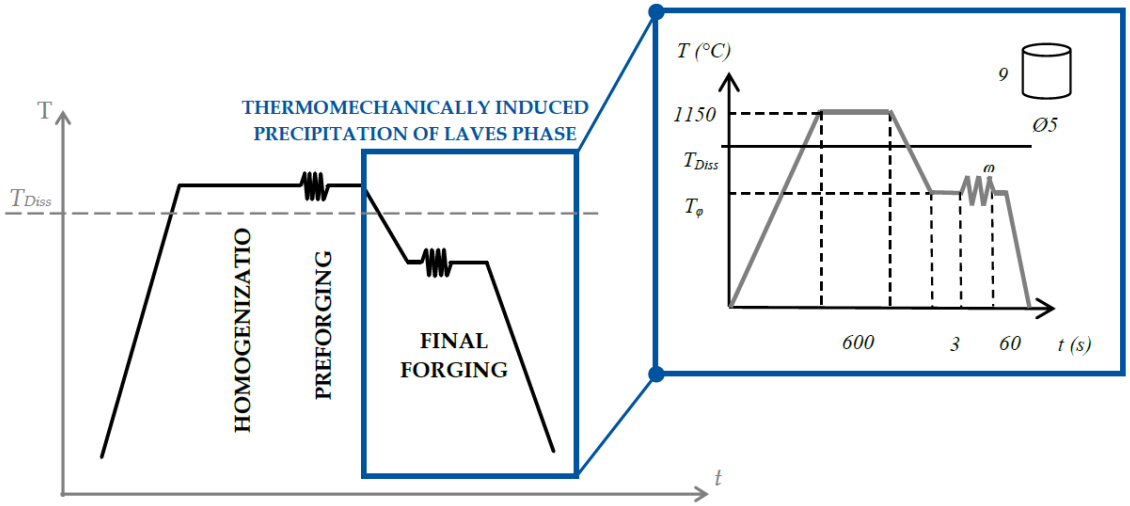

Figure 1. Thermomechanical processing chain applied in the deformation of small-trial-processing specimens for the in-depth investigation of thermomechanically induced precipitation of the strengthening Laves phase. Varying deformation temperatures T_φ (800/850/900 °C) and deformation grades φ (0.25/0.5/1) were applied. T_{Diss} indicates the calculated Laves phase dissolution temperature.

For the mechanical characterization, 15 mm thick plates were prepared from both of the alloys by forging the casted blocks, cutting, soaking (1140 °C/2 h), and multiple rolling (four passes, T: 950–920 °C) with interpass annealing (1085 °C/10 min.) and subsequent water cooling (for details of the applied processing route, named "_4", refer to [6]). All of the rolling passes were carried out below the Laves phase dissolution temperature to prevent excessive grain growth. Interpass annealing was performed above the Laves phase dissolution temperature for a suitably short time to allow stress reduction and diminish grain growth. According to the outlined forging process of the dilatometer specimens, the final rolling pass of the plate materials was performed without prior interpass annealing and below the Laves phase dissolution temperature. Regardless of boron addition, the same procedure was applied for both of the alloys B0 and B55 to ensure one-on-one comparability of the mechanical characterization results.

2.2. Microstructure Analysis

The precipitation behavior was investigated using scanning electron microscopy (SEM)—Zeiss Σigma (Jena, Germany) with an in-lens detector for high-resolution imaging. All SEM samples were examined in a reproducible, polished state. Quantitative particle analysis was performed utilizing the Java-based image processing software ImageJ (version 1.53f). Based on the SEM resolution, all precipitates below 10 nm as well as clearly identifiable inclusions (e.g., niobium oxides) were excluded from further evaluation. The Laves phase area fraction was calculated as a percentage of the area only in the grain interiors without considering the precipitate-free zones. Twenty to forty thousand intragranular particles were analyzed per sample. Regarding the number of particles and the symmetrical angular shape of the precipitates, the area fraction represents a quantitative value that allows statements to be made about the Laves phase precipitation. Since very fine precipitates in high number density occur on the grain boundaries, a quantitative analysis of the mean particle size in this area was impossible to provide due to the overlapping of precipitates. Therefore, a determination of the grain boundary coverage ratio by Laves phase for both investigated alloys was performed. This value represents a ratio of the grain boundary length occupied by Laves phase precipitates relative to the total grain

boundary length. Additionally, light optical microscopy (OM) (Leica Microsystems, Wetzlar, Germany) was carried out to provide an overview of microstructure images, made visible by the Lichtenegger and Bloech (LB) etching method. This is composed of 100 mL of distilled water, 20 g of ammonium hydrogen difluoride, and 0.5 g of potassium sulfide. The hardness was determined using the Vickers method (HV10) (Wolpert, Bretzfeld, Germany) in accordance with the standard [22] at ambient temperature.

2.3. Mechanical Testing

To validate the impact of boron addition on the high-temperature properties of the HiperFer steel, class creep and thermomechanical fatigue experiments were performed. Due to the limited sample size for thermomechanical treatment on the laboratory scale and the comparability with previous research results using the B0 composition, the B55 material was thermomechanically treated in the same way as the non-boron-alloyed B0 composition [4] in the first approach. This means that both alloys in this study were cold-rolled (CR), applying the same procedure [6]. Mechanical testing was performed on the materials in the as-rolled state. Creep testing was performed utilizing cylindrical standard specimens (ø 6.4 × 30 mm^3). The samples were crept at a constant load using lever-arm-type creep machines that were equipped with 3-zone resistance furnaces in laboratory air. The thermomechanical fatigue experiments were carried out on servo-hydraulic fatigue testing systems, applying the inductive heating of cylindrical specimens (ø 6.8 × 15 mm^3) in total strain control in a temperature range from 50 to 650 °C ("out-of-phase-cycle"). The heating and cooling rates during the experiments were held at 10 °C·s^{-1} to minimize creep at temperatures beyond 580 °C. Additionally, no holding time was implemented at the hot end of the cycle.

3. Results and Discussion

3.1. Thermodynamic Simulation

The material concept of the HiperFer steel class is based on precipitation hardening by Laves phase in combination with solid solution strengthening by the high-atom-radius alloying elements niobium and tungsten as well as a coarse-grained ferritic matrix [2,15]. The two examined materials (B0 and B55) were investigated by thermodynamic equilibrium calculations. As shown in the phase amount diagram (Figure 2), the HiperFer material concept consists of the following phases: sigma phase, Laves phase, carbides, and brides. The Laves phase forms in two different variations, which are termed low-temperature Laves phase (LTL) $(Fe,Si,Cr)_2(Nb,W)$ in the stability range up to approximately 750 °C, and high-temperature Laves phase (HTL) $(Fe,Si,Cr)_2(W,Nb)$ up to approximately 1000 °C. The LTL is classified as a metastable phase [5,8]. Due to the significantly slow diffusivity of tungsten atoms compared to niobium atoms, the metastable, niobium-rich LTL preferentially nucleates and grows in the early stages of precipitation. As a result of the diffusion-related "later" availability of the tungsten atoms, the LTL begins to change chemically upon prolonged aging. A continuous tungsten enrichment process during isothermal annealing has already been experimentally observed in the form of two-phase particles with a niobium-rich core and a tungsten-rich shell, as reported in [9,23–25]. The tungsten enrichment of the LTL particles proceeds until the thermodynamically stable chemical composition of the tungsten-rich HTL is reached [5,24,25]. The niobium carbides (NbC) in B0 exhibited high thermodynamic stability, and their dissolution temperature was above 1250 °C. However, due to the low carbon content of <0.01 wt. % and the low phase fraction, they are not of any major relevance. The boron-alloyed steel B55 shows no formation of carbides. On the other hand, the formation of a low amount of chromium borides (Cr_2B) was simulated. The solubility limit of boron in ferrite is limited to 0.004 wt. % at 700 °C and 0.08 wt. % at 900 °C [26].

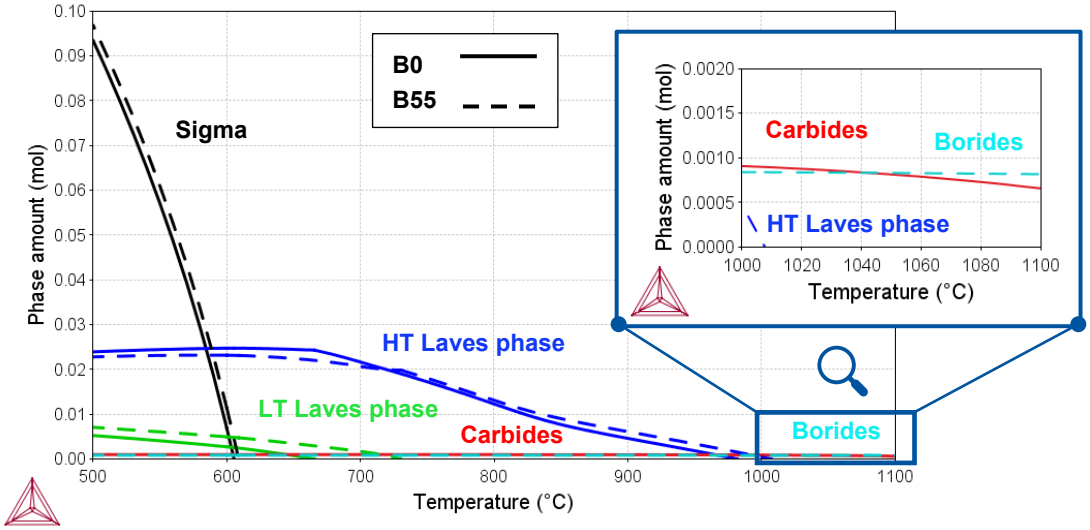

Figure 2. Results of the thermodynamic equilibrium calculation of phase amount in the investigated reference B0 and the boron-alloyed B55 alloy (ThermoCalc, database TCFE8).

The thermodynamic equilibrium calculation was based on the chemical composition of the alloys given in Table 1. The pictured differences in the phase amounts of the (Fe,Cr)-Sigma and the Laves phase are a result of the slight divergence in the chemical composition of the investigated alloys, particularly because of tungsten and niobium (B0: 2.41 W, 0.64 Nb, and B55: 2.35 W, 0.62 Nb in wt. %). The main Laves phase-forming elements niobium and tungsten exhibit a considerable impact on the amount of Laves phase by an infinitesimal increase: Tungsten supports the HTL formation and niobium the LTL [15,17]. Silicon (B0: 0.27 Si and B55: 0.30 Si in wt. %) affects the precipitation kinetics of the Laves phase positively and significantly since it accelerates its formation due to the decreasing solubility of niobium and tungsten in the ferritic matrix [27,28]. Additionally, nucleation of the Laves phase preferentially takes place at segregation regions of silicon and Laves-phase-forming elements [29]. The calculated chemical composition of the HTL as well as the LTL at 650 °C is given in Table 2. Based on the thermodynamic equilibrium calculation results, boron does not participate in the Laves phase-forming process and therefore shows no impact on the Laves phase amount, which is in good agreement with the literature [19,21]. This was additionally verified by a calculation utilizing the nominal chemical composition Fe-17Cr-0.6Nb-2.4W and a 55 ppm boron variation.

Table 2. Calculated chemical composition of the occurring Laves phases at 650 °C (in wt. %; ThermoCalc, database TCFE8).

Alloy	Laves Phase	Si	Cr	Nb	W	Fe
B0	**LTL**	2.4	2.2	35.2	16.1	44.1
	HTL	0.3	6.7	12.3	45.9	34.8
B55	**LTL**	2.8	2.0	35.3	15.7	44.2
	HTL	0.4	6.8	12.1	46.4	34.3

3.2. Precipitation Behavior—Grain Interiors

The thermomechanical treatment of the investigated alloys was performed at different temperatures. The microstructure OM overview images at a constant deformation grade of 0.5 and increasing deformation temperature are shown in Figure 3. The obvious differences in the microstructure can be supported by the intragranular particle analysis results based on the SEM images. Figure 4 depicts the influence of the deformation temperature at a constant deformation grade of 0.5 on the mean particle size in the grain interior and the corresponding Laves phase area fraction.

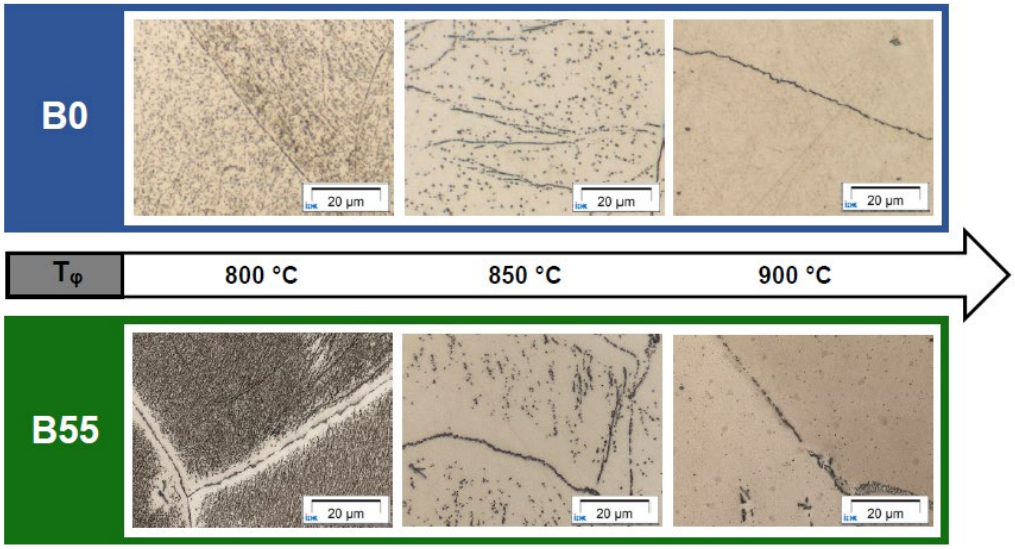

Figure 3. Impact of the deformation temperature of 800 °C/850 °C/900 °C with a 0.5 deformation grade of the reference B0 in comparison to the boron-alloyed B55 steel.

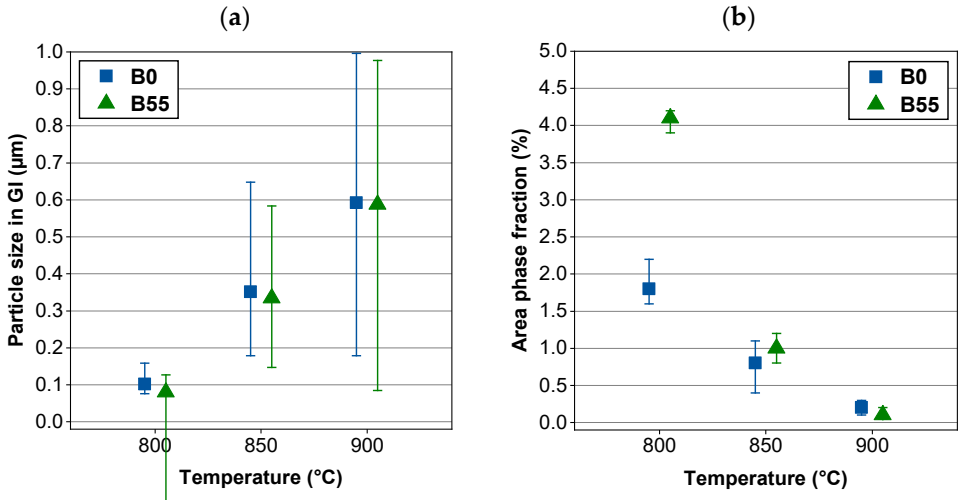

Figure 4. Quantitative particle analysis results: (**a**) mean particle size in the grain interior (GI) and (**b**) area phase fraction after thermomechanical treatment of the reference B0 and the boron-alloyed B55 steel with varying deformation temperature (800/850/900 °C; deformation grade, 0.5).

In both of the alloys, the precipitation of a multitude of fine (<0.1 µm) Laves phase particles was achieved at the deformation temperature of 800 °C. An increase in forging temperature to 850 °C and 900 °C resulted in an acceleration of the diffusion-related growth and coarsening processes by decreasing the driving force. Correspondingly, the formation of significantly coarser Laves phase particles (>0.5 µm at 900 °C) can be observed along with a reduced area fraction below 0.5%. The highest Laves phase area fraction of 4.1% was achieved in B55 after thermomechanical treatment at 800 °C and a deformation grade of 0.5. A very fine, homogeneously dispersed Laves phase precipitation with a mean particle size of 0.08 µm was formed under these conditions. The boron-alloyed B55 steel exhibited slightly finer precipitates and comparable area phase fraction than the alloy B0. Solely at the deformation temperature of 800 °C, a significant area phase fraction difference of intragranular Laves phase precipitates (B0: 1.8%, B55: 4.1%) was observed.

Due to the rapid deformation process, the acceleration in kinetics based on the slightly higher silicon content in B55 shows major importance in this process at 800 °C compared to the B0 alloy. Additionally, due to the presence of particle-free zones in B55 (see Figure 3)

and therefore depletion of the Laves phase-forming elements in these areas, the grain interior area is smaller and the alloying atoms number is significantly higher in comparison to the alloy B0.

By increasing the deformation grade and therefore creating additional nucleation sites in the form of dislocations, a tendency toward finer precipitation can be observed. The quantitative analysis results of intragranular mean particle size and area phase fraction are displayed in Figure 5. The reference B0 alloy demonstrated higher sensitivity to the variation in the deformation grade than B55. The B55 alloy exhibits a slightly decreasing tendency. Increasing the deformation grade from 0.25 to 0.5 caused finer precipitation. B0 exhibited a decrease in mean particle size from 0.17 µm to 0.10 µm, whereas B55 from 0.10 µm to 0.08 µm. This higher sensitivity of B0 to the deformation grade can be explained by the lower silicon content. The acceleration of precipitation kinetics due to the dislocations serving as nucleation sites exhibits a more significant impact because of the lower number of silicon segregation areas compared to B55. In other words, the lower number of created nucleation sites (dislocations) in B55 can be compensated by accelerated kinetics due to increased silicon content. Even an infinitesimally higher silicon content results in a considerable promotion of the fine Laves phase precipitation [27,28].

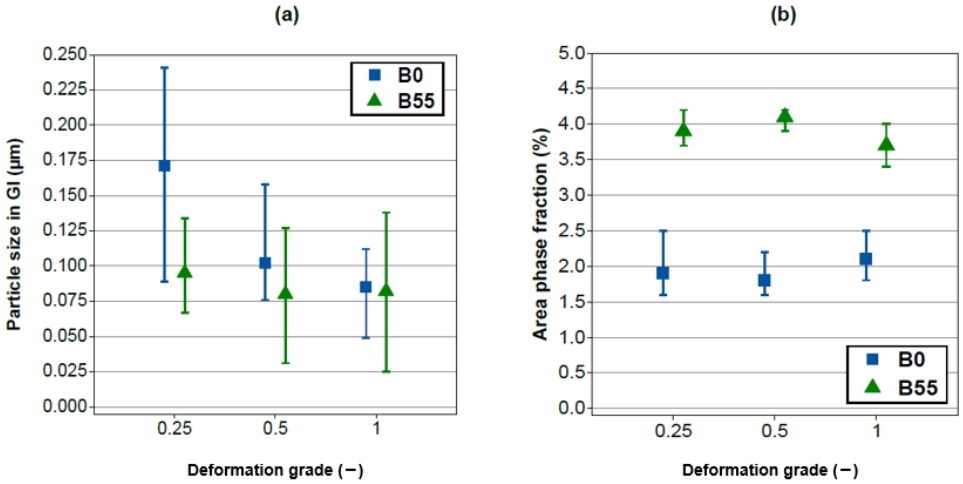

Figure 5. Quantitative particle analysis results: (**a**) mean particle size in the grain interior (GI) and (**b**) area phase fraction after thermomechanical treatment of the reference B0 and the boron-alloyed B55 steel with deformation grades from 0.25 to 1 at an 800 °C deformation temperature.

The described results for the quantitative intragranular particle analysis of the grain interior Laves phase precipitation can be validated by OM overview images with a constant deformation temperature of 800 °C and increasing deformation grade, as shown in Figure 6. Significantly broader precipitate-free zones can be observed in B55. These alloying element-depleted areas imply changed diffusion conditions due to the boron addition as well as a different content of Laves phase-forming elements in the grain interiors. Consequently, higher silicon content in combination with a dissimilar content of Laves phase-forming elements in the grain interiors results in a higher area phase fraction in B55. The achieved Laves phase area fraction in the grain interior remains constant (B0: ~1.9%, B55: ~3,9%) in both investigated alloys with variations in deformation grade.

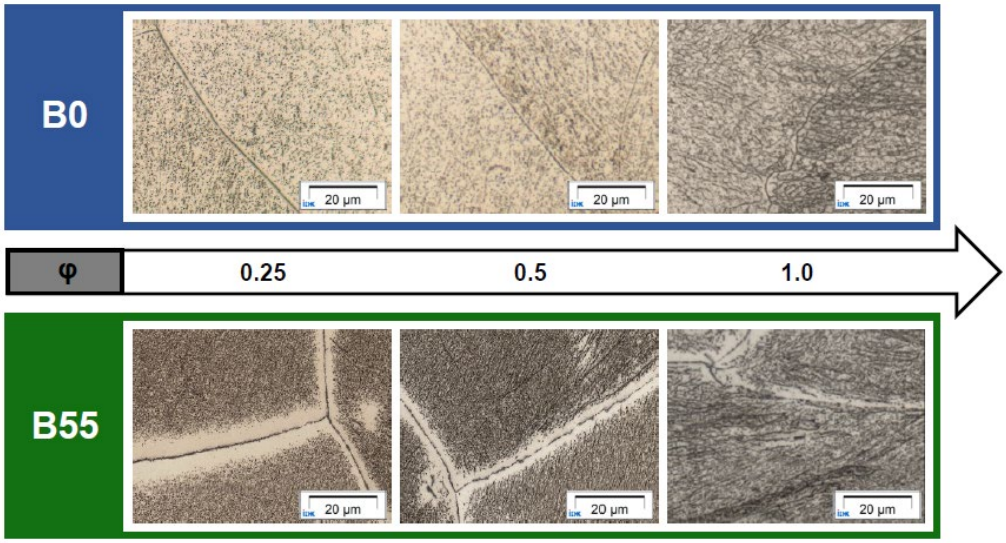

Figure 6. Impact of the deformation grade variation (0.25/0.5/1) at an 800 °C deformation temperature on precipitation in the reference B0 in comparison to the boron-alloyed B55 steel.

3.3. Precipitation Behavior—Grain Boundaries

Based on the high diffusivity of boron and the fact that boron has a strong tendency to segregate to grain boundaries [30–32], the boron effect in HiperFer steels can be further demonstrated by a different precipitation behavior at the grain boundaries. Figure 6 contains light optical overview micrographs of both investigated alloys after thermomechanical treatment at 800 °C with dependency on increasing deformation grade. The observed Laves phase precipitates at the grain boundaries in the boron-alloyed B55 steel are finer and higher in number than in the reference alloy B0. It has been reported that boron segregation to the grain boundaries promotes the precipitation process [18,19,33]. Furthermore, a strong reduction in the Ostwald ripening process of precipitates is achieved in this area [19]. The accumulation of boron at the grain boundaries occurs predominantly by nonequilibrium segregation (at a cooling rate of 150 °C·s^{-1}). Due to the changed chemical composition in the grain boundary area, the diffusion processes also differ with respect to the grain interior [34]. Since very fine precipitates in high number density occur on the grain boundaries, a quantitative analysis of the mean particle size in this area was impossible due to the overlapping of the precipitates. Therefore, a comparison of the grain boundary coverage ratio by Laves phase for both investigated alloys is given in Figure 7. The fraction of the grain boundary length covered by Laves phase is higher in the boron-alloyed steel B55 despite the observed lower mean particle size. The maximum value of the grain boundary coverage ratio of 76% has been reached with a deformation grade of 0.25 at a deformation temperature of 800 °C. For austenitic heat-resistant steels, it has been reported that the strengthening effect of Laves phase (Fe_2Nb) depends on this grain boundary coverage ratio [18]. Thus, higher Laves phase occupation of the grain boundaries results in better creep resistance [18].

Due to the changed diffusion conditions by segregated boron, the transport of Laves-phase-forming elements to the grain boundaries is accelerated [18,19]. Furthermore, the grain boundary is substantially occupied by boron atoms, and, therefore, the number of nucleation sites for the Laves phase increases [19,33]. Consequently, the creation of a higher number of nucleation sites is promoted and fine Laves phase particles can be formed.

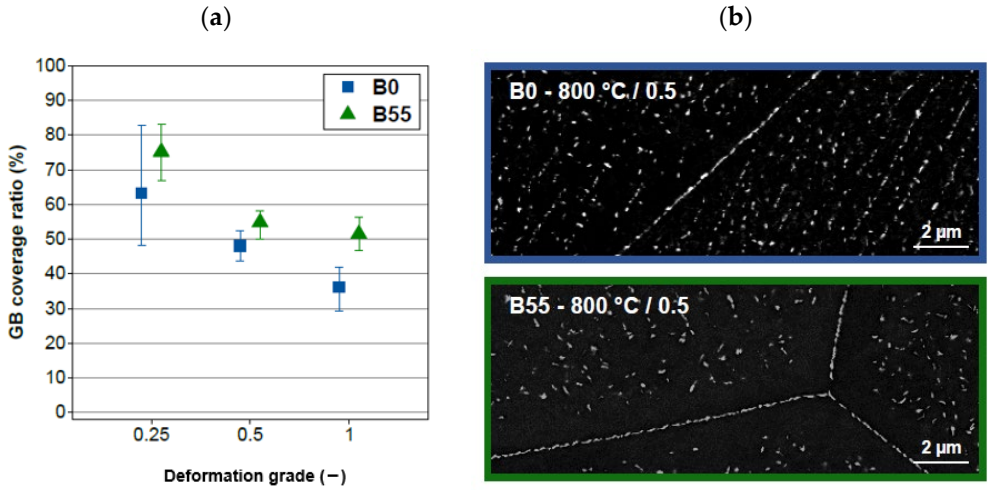

Figure 7. (**a**) Grain boundary coverage ratio (Laves phase precipitates occupied grain boundary length relative to the total length) after thermomechanical treatment with varying deformation grades of 0.25/0.5/1 at an 800 °C deformation temperature. (**b**) SEM-BSE precipitation images (800 °C with 0.5 deformation grade).

Comparing the microstructures of the two investigated alloys, a significant difference in the precipitation behavior along the grain boundaries can be observed (see Figure 6). The boron-alloyed steel B55 exhibits distinct precipitation-free zones in contrast to the reference alloy B0. The broader precipitate-free zones correspond to the accelerated transport of alloying elements to the grain boundaries, caused by boron segregation. The following, diffusion-related growth and coarsening processes of the formed Laves phase particles are retarded by the presence of precipitate-free zones and, accordingly, the increased transport distance. Furthermore, the width of the precipitate-free zone decreases by increasing the deformation grade in B55 (see Figure 6). According to the literature, a different formation mechanism of precipitate-free zones occurs as a result of boron addition [33,34]. The precipitate-free zones in boron-free alloys are related to the depletion of precipitation-forming elements as a consequence of the accelerated diffusion of atoms to the grain boundaries. On the contrary, particle-free zones in boron-alloyed steels are formed due to the accelerated diffusion processes as well as the changed segregation degree and diffusivity of other elements [33–37].

In general, the predominant nonequilibrium segregation of boron at grain boundaries depends primarily on the cooling rate and the starting temperature [31]. Considering the thermomechanical treatment, the degree of boron segregation shows a dependency on further parameters such as dislocation density, grain boundary velocity, or recrystallization temperature [20]. The dislocations absorbed into grain boundaries are not removed immediately; therefore, the grain boundary thickness and distortion are influenced [20]. Correspondingly, the segregation degree of boron increases. Additionally, the thermomechanical treatment creates a partially elongated grain structure. Due to the coarse grain size of HiperFer steels in general, the significant inhomogeneity of the grains as well as the small size of the dilatometer samples, a quantitative comparison of the grain size is not possible. The microstructure, including grain boundary length and grain size, also determines the degree of segregation of boron, limiting dissolution, boride formation, and the resulting availability of free boron atoms. However, based on the different deformation grades and, therefore, distinct dislocation density as well as nonidentical grain boundary length, the boron distribution at the grain boundaries can differ. As a result, no constant segregations and diffusivity conditions are created by varying the deformation grades near the grain boundaries resulting in a clear impact of the deformation grade on the width of precipitate-free zones.

3.4. Mechanical Properties

The hardness results, indicating mechanical properties, are displayed in Figure 8. Due to thermomechanical processing, hardness is increased in comparison to the solution-annealed condition. Based on this comparison, the strengthening effect of the treatment as well as the chemical composition can be assessed. The hardness of B0 in the precipitation-free state after dissolution annealing is higher than the hardness of B55. This slight difference is caused by a higher solid solution strengthening effect in the reference steel B0 because of the higher contents of the high-atom-radius elements tungsten and niobium. As expected, thermomechanical treatment increases the hardness values based on the combination of precipitation and work hardening. By increasing the deformation temperature, coarser precipitates are formed. As a result of the coarser precipitates and the corresponding larger particle distances, a noticeable decrease in the precipitation strengthening effect and therefore in hardness can be observed. Moreover, the promotion of diffusion-induced softening mechanisms by higher deformation temperatures has to be considered. Increasing the deformation grade creates a higher density of dislocations and increases the number of nucleation sites of the Laves phase particles. Accordingly, a higher effect of precipitation as well as deformation strengthening can be observed. Independent of the treatment parameters, B55 exhibits higher hardness values in comparison to B0. These results agree with the microstructural observations described above. A finer Laves phase precipitation, higher area phase fraction, and an observably higher density were found in B55. Correspondingly, a higher precipitation strengthening effect was achieved.

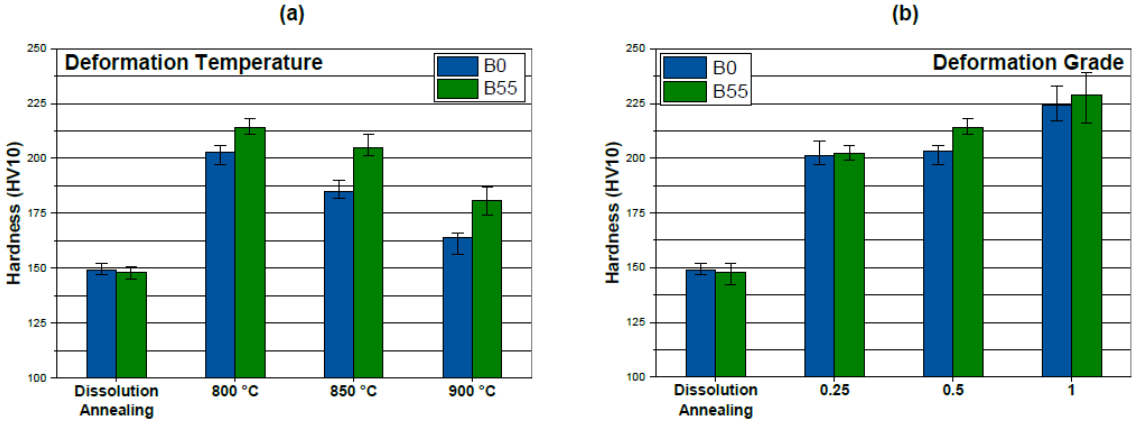

Figure 8. HV10 hardness results of the thermomechanically treated alloys B0 and B55 in comparison to the precipitate-free microstructure after solution annealing in dependence on (**a**) deformation temperature with a 0.5 deformation grade and (**b**) a deformation grade at an 800 °C deformation temperature.

3.5. High-Temperature Mechanical Properties

The outlined microstructural differences demonstrate a decent impact on the creep properties of the trial steels. Using a test stress of 120 MPa (rupture times t_R: B0: 2.010 h; B55: 1.788 h, Figure 9a), the B55 alloy performs within a −5% scatter band (in terms of stress, Figure 9b) of the B0-alloy fit line. At 100 MPa (t_R: B0: 5.334 h; B55: 4.113 h) and 70 MPa (t: B0: 32.335 h, in progress; t_R: B55: 15.736 h) it undershoots this range (Figure 9b). The transition from the primary to the tertiary creep stage (HiperFer steels yield minimally to an almost absent secondary creep [6]) obviously appears much earlier in the case of alloy B55.

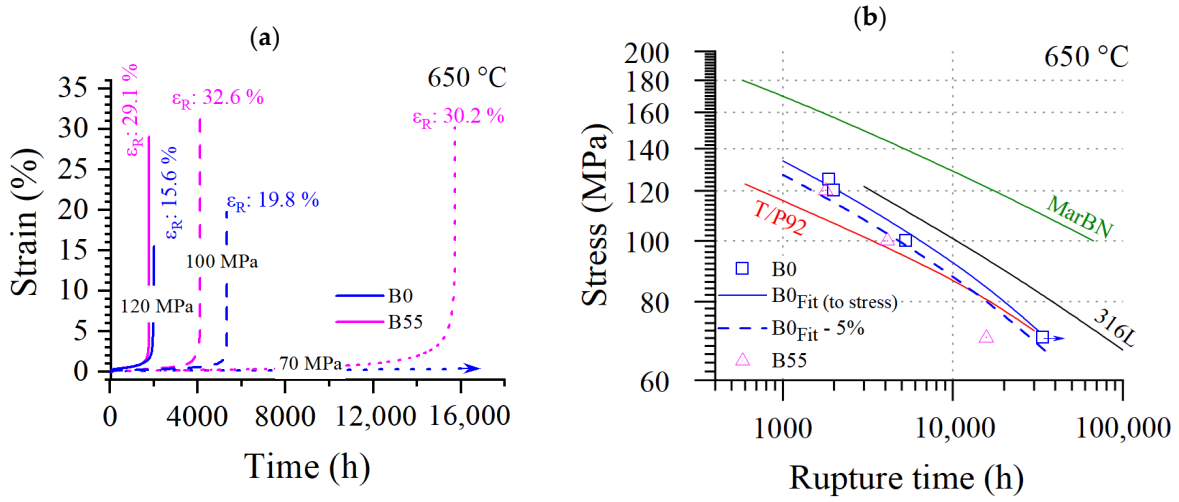

Figure 9. Creep curves (650 °C) of the trial steels. (**a**) Stress–rupture performance relative to the state-of-the-art structural steels used for power engineering (blue: B0, magenta: B55; solid lines: 120 MPa, dashed lines: 100 MPa, dotted lines: 70 MPa). (**b**) The 70 MPa experiment with the B0-alloy is still in progress—the fit line, for this reason, is still premature. Creep data were taken from B0 [6], MarBN [38], T/P92, 316L [39].

On the other hand, B-alloying leads to an increase in creep rupture elongation at all the investigated stress levels/rupture times (Figure 9a). Both these findings are in good accordance with the previously outlined microstructural differences because creep damage of HiperFer steels is mainly governed by the accumulation of creep deformation within creep soft precipitate-free zones at grain boundaries [9,10]. The boron in B55 leads to creep in stronger grain interiors (because of smaller and more numerous Laves phase precipitates), stronger grain boundaries (because of boron segregation), and higher precipitate-free zone widths. In turn, intragranular creep deformation and grain boundary slip decrease, which leads to increased localization of creep deformation within the wider precipitate-free zones. This, on the one hand, enables increased rupture elongation; however, on the other hand, it also causes premature damage and failure.

Improved creep damage and rupture performance of the boron-alloyed B55 steel may be accessible through reduced precipitate-free zone widths based on altered thermomechanical processing. The potential reduction in creep rupture elongation may be counterbalanced by tuned grain size.

The HiperFer steel grades were designed for improved fatigue resistance [8] at high temperatures, based on improved stability of the grain structure [40–42] and active crack obstruction by the thermomechanically induced precipitation of Laves phase particles in front of crack tips [7,43,44]. The thermomechanical fatigue life behavior of the reference HiperFer steel B0 and the boron-alloyed variant B55 in comparison to the relevant AFM grades and the austenitic, stainless steel 316L is depicted in Figure 10.

As with most materials, the fatigue of HiperFer-like steels is a predominantly transgranular phenomenon [41,44]. The wider precipitate-free zones at grain boundaries, which limit the creep resistance of B55 (Figure 9) do not play a significant role in fatigue performance. Consequently, the boron-alloyed B55 batch performs similarly to the boron-free material B0.

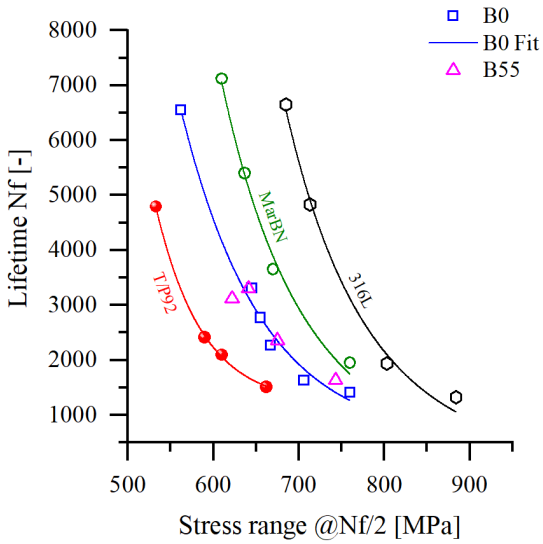

Figure 10. Thermomechanical fatigue testing (ΔT: 50–650 °C, dT/dt: 10 Ks^{-1}, $\varepsilon_{mech.} = -1$ to $-0.48 \cdot \varepsilon_{therm.}$, no holding times at $T_{min.}/T_{max.}$) results of the alloys B0 and B55 in comparison to advanced ferritic–martensitic grades (AFM: grade 92, MarBN) and stainless, austenitic steel (316L). B0, T/P92, MarBN, and 316L data from [7].

4. Conclusions

A review of thermomechanically induced Laves phase precipitation in boron-free and boron-alloyed HiperFer steels of the nominal chemical composition Fe-17Cr-0.6Nb-2.4W has been provided. An acceleration of Laves phase precipitation at grain boundaries due to the added boron in HiperFer steels has been observed. In this new class of steels, the availability of solute, grain-boundary-active boron atoms is promoted by the practical absence of nitrogen and carbon and the nonparticipation of boron in $(Fe,Cr,Si)_2(Nb,W)$ Laves phase formation. Independent of the thermomechanical treatment parameters, the tendency of early boron segregation at grain boundaries is beneficial for the refinement of intragranular Laves phase precipitates. Furthermore, boron addition boosts grain boundary coverage by Laves phase precipitates.

The significant impact of boron on the diffusion conditions in the area next to the grain boundaries has been demonstrated by a distinct increase in precipitation-free zone (PFZ) widths with the addition of boron. The widths of these PFZs play an important role in creep damage and failure of HiperFer steel. Boron alloying causes wider PFZs, which in turn leads to increased strain accumulation within these. Therefore, creep rupture deformation is improved; however, creep failure appears prematurely in comparison to the boron-free parent alloy. The thermomechanical fatigue resistance is not affected by boron alloying because fatigue is a mainly transgranular phenomenon.

Furthermore, PFZ formation exhibits a dependency on the grade of deformation during processing. The further optimization of thermomechanical processing toward increased creep rupture deformation and creep rupture time seems possible, for this reason, if a suitable combination of grain size and PFZ width is found.

Author Contributions: Conceptualization, J.P. and B.K.; methodology, J.P. and B.K.; investigation, J.P., D.W. and B.K.; writing—original draft preparation, J.P.; writing—review and editing, D.W. and B.K.; visualization, J.P., D.W. and B.K.; supervision, W.B.; project administration, J.P. and B.K. All authors have read and agreed to the published version of the manuscript.

Funding: IEHK's contribution was funded by Deutsche Forschungsgemeinschaft (DFG), grant number 631895. IEK-2´s contribution was funded by the German Helmholtz Society Framework Programme "Energy Efficiency, Materials, and Resources" and the German Ministry of Education and Research, under grant number 03EK3032.

Data Availability Statement: All available data are presented in this paper.

Acknowledgments: The authors gratefully acknowledge the scientific cooperation between the Institute of Energy and Climate Research (IEK), Microstructure and Properties of Materials (IEK-2), Forschungszentrum Jülich GmbH, and the Steel Institute at RWTH Aachen (IEHK) as well as the support of the technical staff in performing the experiments and microstructural investigations.

Conflicts of Interest: The authors declare no conflict of interest.

References

1. Kuhn, B.; Talík, M. HiperFer-High performance ferritic steels. In Proceedings of the 10th Liége Conference on Materials for Advanced Power Engineering, Liége, Belgium, 15–17 September 2014; pp. 14–17.
2. Kuhn, B.; Talík, M.; Zurek, J.; Beck, T.; Quadakkers, W.J.; Singheiser, L.; Hattendorf, H. Development of high chromium ferritic steels strengthened by intermetallic phases. *Mater. Sci. Eng. A* **2014**, *594*, 372–380. [CrossRef]
3. Talík, M.; Lopez Barrilao, J.; Kuhn, B. High Temperature Mechanical Properties of a 17wt% Cr High Performance Ferritic (HiperFer) Steel Strengthened by Intermetallic Laves Phase Particles. In Proceedings of the 9th International Charles Parsons Turbine and Generator Conference, Loughborough, UK, 15–17 September 2015.
4. Fan, X.; Kuhn, B.; Pöpperlová, J.; Bleck, W.; Krupp, U. Thermomechanically Induced Precipitation in High-Performance Ferritic (HiperFer) Stainless Steels. *Appl. Sci.* **2020**, *10*, 5713. [CrossRef]
5. Pöpperlová, J. Verformungsinduzierte Ausscheidung Intermetallischer Laves-Phase in Hochwarmfesten Ferritischen Stählen. Ph.D. Thesis, RWTH Aachen University, Aachen, Germany, 2021.
6. Kuhn, B.; Talik, M. Impact of Processing on the Creep Properties of High Performance Ferritic (HiperFer) Steels. *Metals* **2022**, *12*, 1459. [CrossRef]
7. Kuhn, B.; Talik, M.; Fischer, T.; Fan, X.; Yamamoto, Y.; Barrilao, J.L. Science and Technology of High Performance Ferritic (HiperFer) Stainless Steels. *Metals* **2020**, *10*, 463. [CrossRef]
8. Lopez Barrilao, J.; Kuhn, B.; Wessel, E. Identification, size classification and evolution of Laves phase precipitates in high chromium, fully ferritic steels. *Micron* **2017**, *101*, 221–231. [CrossRef] [PubMed]
9. Kuhn, B.; Fischer, T.; Fan, X.; Talík, M.; Aarab, F.; Yamamoto, Y. HiperFer—Weiterentwicklungs- und Anwendungspotenziale. In Proceedings of the 43 FVWHT Vortragsveranstaltung Langzeitverhalten Warmfester Stähle und Hochtemperaturwerkstoffe, Düsseldorf, Germany, 27 November 2020.
10. Kuhn, B.; Jimenez, C.A.; Niewolak, L.; Hüttel, T.; Beck, T.; Hattendorf, H.; Singheiser, L.; Quadakkers, W. Effect of Laves phase strengthening on the mechanical properties of high Cr ferritic steels for solid oxide fuel cell interconnect application. *Mater. Sci. Eng. A* **2011**, *528*, 5888–5899. [CrossRef]
11. Mangen, W.; Nembach, E. The effect of grain size on the yield strength of the γ'-hardened superalloy NIMONIC PE16. *Acta Metall.* **1989**, *37*, 1451–1463. [CrossRef]
12. Krol, T.; Baither, D.; Nembach, E. The formation of precipitate free zones along grain boundaries in a superalloy and the ensuing effects on its plastic deformation. *Acta Mater.* **2004**, *52*, 2095–2108. [CrossRef]
13. Kawabata, T.; Izumi, O. Ductile fracture in the interior of precipitate free zone in an Al-6.0% Zn-2.6% Mg alloy. *Acta Metall.* **1976**, *24*, 817–825. [CrossRef]
14. Krol, T.; Baither, D.; Nembach, E. Quantification of the detrimental effects of precipitate free zones on the yield strength of a superalloy. *Scr. Mater.* **2003**, *48*, 1189–1194. [CrossRef]
15. Fan, X.; Kuhn, B.; Pöpperlová, J.; Bleck, W.; Krupp, U. Compositional Optimization of High-Performance Ferritic (HiperFer) Steels—Effect of Niobium and Tungsten Content. *Metals* **2020**, *10*, 1300. [CrossRef]
16. Froitzheim, J.; Meier, G.; Niewolak, L.; Ennis, P.; Hattendorf, H.; Singheiser, L.; Quadakkers, W. Development of high strength ferritic steel for interconnect application in SOFCs. *J. Power Sources* **2008**, *178*, 163–173. [CrossRef]
17. Pöpperlová, J.; Fan, X.; Kuhn, B.; Bleck, W.; Krupp, U. Impact of Tungsten on Thermomechanically Induced Precipitation of Laves Phase in High Performance Ferritic (HiperFer) Stainless Steels. *Appl. Sci.* **2020**, *10*, 4472. [CrossRef]
18. Chen, S.W.; Zhang, C.; Xia, Z.X.; Ishikawa, H.; Yang, Z.G. Precipitation behavior of Fe2Nb Laves phase on grain boundaries in austenitic heat resistant steels. *Mater. Sci. Eng. A* **2014**, *616*, 183–188. [CrossRef]
19. Abe, F. Effect of Boron on Microstructure and Creep Strength ofAdvanced Ferritic Power Plant Steels. *Procedia Eng.* **2011**, *10*, 94–99. [CrossRef]
20. Jahazi, M.; Jonas, J. The non-equilibrium segregation of boron on original and moving austenite grain boundaries. *Mater. Sci. Eng. A* **2002**, *335*, 49–61. [CrossRef]
21. Abe, F. Precipitate design for creep strengthening of 9% Cr tempered martensitic steel for ultra-supercritical power plants. *Sci. Technol. Adv. Mater.* **2008**, *9*, 013002. [CrossRef] [PubMed]
22. *German Standard DIN EN ISO 6507-1*; Metallic Materials—Vickers Hardness Test—Part 1: Test Method. Beuth: Berlin, Germany, 2018.
23. Niewolak, L.; Savenko, A.; Grüner, D.; Hattendorf, H.; Breuer, U.; Quadakkers, W.J. Temperature Dependence of Laves Phase Composition in Nb, W and Si-Alloyed High Chromium Ferritic Steels for SOFC Interconnect Applications. *J. Phase Equilibria Diffus.* **2015**, *36*, 471–484. [CrossRef]

24. Lopez, B.; Jennifer, K. Microstructure Evolution of Laves Phase Strengthened Ferritic Steels for High Temperature Application. Ph.D. Thesis, RWTH Aachen University—FZ Jülich, Aachen, Germany, 2016.
25. Nabiran, N.; Klein, S.; Weber, S.; Theisen, W. Evolution of the Laves Phase in Ferritic Heat-Resistant Steels During Long-term Annealing and its Influence on the High-Temperature Strength. *Metall. Mater. Trans. A* **2015**, *46*, 102–114. [CrossRef]
26. Filonenko, N. Solubility of Boron and Carbon in Ferrite of the Fe-B-C System Alloys. *East Eur. J. Phys.* **2019**, *2*, 52–57. [CrossRef]
27. Aghajani, A.; Richter, F.; Somsen, C.; Fries, S.; Steinbach, I.; Eggeler, G. On the formation and growth of Mo-rich Laves phase particles during long-term creep of a 12% chromium tempered martensite ferritic steel. *Scr. Mater.* **2009**, *61*, 1068–1071. [CrossRef]
28. Kato, Y.; Ito, M.; Kato, Y.; Furukimi, O. Effect of Si on Precipitation Behaviour of Nb-Laves Phase and Amount of NB in Solid Solution at Elevated Temperature in High Purity 17% Cr-0.5% Nb Steels. *Mater. Trans.* **2010**, *51*, 1531–1535. [CrossRef]
29. Isik, M.; Kostka, A.; Eggeler, G. On the nucleation of Laves phase particles during high-temperature exposure and creep of tempered martensite ferritic steels. *Acta Mater.* **2014**, *81*, 230–240. [CrossRef]
30. Karlsson, L.; Noden, H. Grain Boundary Segregation of Boron. An Experimental and Theoretical Study. *J. Phys. Colloq.* **1986**, *47*, 257–262. [CrossRef]
31. Karlsson, L.; Noden, H.; Odelius, H. Non-equilibrium grain boundary segregation of boron in austenitic stainless steel—I. Large scale segregation behaviour. *Acta Metall.* **1988**, *36*, 1–12. [CrossRef]
32. Karlsson, L.; Nordén, H. Overview no. 63 Non-equilibrium grain boundary segregation of boron in austenitic stainless steel-II. Fine scale segregation behaviour. *Acta Metall.* **1988**, *36*, 13–24. [CrossRef]
33. Osanai, T.; Sekido, N.; Yonemura, M.; Maruyama, K.; Takeuchi, M.; Yoshimi, K. Evolution of boron segregation during tempering in B doped 9% Cr ferritic steel. *Mat. Charact.* **2021**, *177*, 111192. [CrossRef]
34. Karlsson, L.; Noden, H. Non-equilibrium grain boundary segregation of boron in austenitic stainless steel-IV. Precipitation behaviour and distribution of elements at grain boundaries. *Acta Metall.* **1988**, *36*, 35–48. [CrossRef]
35. Suzuki, S.; Obata, M.; Abiko, K.; Kimura, H. Effect of carbon on the grain boundary segregation of phosphorus in α-iron. *Scr. Metall.* **1983**, *17*, 1325–1328. [CrossRef]
36. Liu, C.M.; Nagoya, T.; Abiko, K.; Kimura, H. Effect of boron on the grain boundary segregation of phosphorus and inter-granular fracture in high-purity Fe-0.2 Pct P-B alloy. *Metall. Trans. A* **1992**, *23*, 263–269. [CrossRef]
37. Paju, M.; Viefhaus, H.; Grabke, H.J. Phosphorus segregation in austenite in Fe-P-C, Fe-P-B and Fe-P-C-B alloys. *Steel Res.* **1988**, *59*, 336–343. [CrossRef]
38. Abtoss, K.G.; Nitsche, A.; Mayr, P.; Schlacher, C.; Gonzales, V.; Aguero, A. Experience with 9Cr3W3CoVNbBN steel in terms of welding, creep and oxidation. In Proceedings of the 8th International Conference on Advances in Material Technology for Fossil Power Plants, Albufeira, Portugal, 11–14 October 2016.
39. ECCC Datasheets 2014. ASTM Grade 92. 2014. Available online: https://pdfslide.net/documents/eccc-data-sheets-2014-i2r001.html?page=6 (accessed on 19 January 2023).
40. Kuhn, B.; Lopez Barrilao, J.; Fischer, T. „Reactive" Microstructure, the Key to Cost-Effective, Fatigue-Resistant High-Temperature Structural Materials. In Proceedings of the Joint EPRI-123HiMAT International Conference on Advances in High-Temperature Materials, Nagasaki, Japan, 21–25 October 2019; pp. 1–10.
41. Kuhn, B.; Lopez Barrilao, J.; Fischer, T. Impact of Thermomechanical Fatigue on Microstructure Evolution of a Ferrit-ic-Martensitic 9 Cr and a Ferritic, Stainless 22 Cr Steel. *Appl. Sci.* **2020**, *10*, 6338. [CrossRef]
42. Fischer, T.; Kuhn, B.; Rieck, D.; Schulz, A.; Trieglaff, R.; Wilms, M.B. Fatigue Cracking of Additively Manufactured Materials—Process and Material Perspectives. *Appl. Sci.* **2020**, *10*, 5556. [CrossRef]
43. Blinn, B.; Görzen, D.; Fischer, T.; Kuhn, B.; Beck, T. Analysis of the Thermomechanical Fatigue Behavior of Fully Ferritic High Chromium Steel Crofer® 22H with Cyclic Indentation Testing. *Appl. Sci.* **2020**, *10*, 6461. [CrossRef]
44. Fischer, T.; Kuhn, B. Active Crack Obstruction Mechanisms in Crofer® 22H at 650 °C. *Materials* **2022**, *15*, 6280. [CrossRef]